Oral Science International 15 (2018) 41–47

Contents lists available at ScienceDirect

Oral Science International

journal homepage: www.elsevier.com/locate/osi

Review

Proteomics pattern associated with gingival oral squamous cell carcinoma and epulis: A case analysis

Francesco Papa[a], Rosa Anna Siciliano[b], Francesco Inchingolo[c], Maria Fiorella Mazzeo[b], Salvatore Scacco[a], Rosa Lippolis[d,*]

[a] Department of Basic Medical Sciences, Neurosciences and Sense Organs, University Aldo Moro, Bari, Italy
[b] Institute of Food Sciences, National Research Council (CNR), Avellino, Italy
[c] Department of Interdisciplinary Medicine, University Aldo Moro, Italy
[d] Institute of Biomembranes and Bioenergetics, Italian National Research Council (CNR), Bari, Italy

ARTICLE INFO

Article history:
Received 7 June 2017
Received in revised form
24 November 2017
Accepted 5 December 2017
Available online 1 February 2018

Keywords:
Biomarkers
Proteomic analysis
Oral squamous cell carcinoma

ABSTRACT

Objectives: Oral squamous cell carcinoma (OSCC) is the most common epithelial malignant neoplasm affecting the oral cavity. OSCC can mimic oral lesions of inflammatory origin with benign features, often leading to delay in diagnosis and treatment. Early detection is important to greatly increase the chances of a successful treatment. The present study reports a proteomic analysis of a gingival oral squamous cell carcinoma (G-OSCC) and an epulis.

Materials and methods: Normal mucosae tissue, G-OSCC tissue, and epulis tissue as a comparative sample of benign nature were collected and immediately frozen in liquid nitrogen. Tissue-extracted proteins were separated by two-dimensional gel electrophoresis and subjected to image analysis. Proteins that showed a significant difference in the expression level in the G-OSCC tissue were identified by the nano-ESI-HPLC-MS/MS experiment and database searchi.

Results and conclusion: The proteomic analysis of G-OSCC tissue enabled the identification of proteins that are potentially related to the disease; these proteins can be considered as signature molecules for diagnostic and prognostic tumor markers.

Contents

Abbreviations: OSCC, oral squamous cell carcinomas; G-OSCC, gingival oral squamous cell carcinoma; 2-DE, two-dimensional electrophoresis; CHAPS, 3-[(3-cholamidopropyl) dimethylammonio]-1-propanesulfonate; DTT, dithiothreitol; LC-ESI-MS/MS, liquid chromatography–electrospray ionization–tandem mass spectrometry.

* Corresponding author at: National Research Council (CNR), C/o Department of Basic Medical Sciences, Neurosciences and Sense Organs, P.zza Giulio Cesare 11, 70124 Bari, Italy.
E-mail address: r.lippolis@ibbe.cnr.it (R. Lippolis).

https://doi.org/10.1016/S1348-8643(17)30044-7
1348-8643/

1. Introduction

The majority of cancers in the oral cavity are oral squamous cell carcinomas (OSCC) [1], a multifactorial disease that arises from the stratified squamous epithelium lining the oral mucosa [2–4]. The tumor originates by morphological cell transformation, often through clinically benign precancerous lesions and develops according to their potential of neoplastic transformation [5–9]. Gingival oral squamous cell carcinoma (G-OSCC), classified as a subset of OSCC, is a relatively rare malignant carcinoma of the oral cavity, representing less than 10% of diagnosed intraoral carcinomas. The etiology of OSCC remains unknown, but it is established that the disease is associated with a variety of risk factors, in particular smoking and heavy alcohol use [10]. OSCC involves a series of mutations that result in the selective growth of mutated cells replacing normal cells in a specific region [11]. Because of its close proximity to the teeth and periodontium, G-OSCC can mimic other tooth-related lesions, especially those of inflammatory origin. Clinical presentation of G-OSCC can be quite variable, and hence, it is misdiagnosed as benign tumor or as inflammatory response. At present, diagnosis of oral cancer is mainly based on clinical oral examination. Histopathology is an adjuvant technique in identifying oral tumor or malignant transformation of oral lesions. The conventional diagnostic methods alone are, however, not sufficient to support early diagnosis of the disease and differential diagnosis with respect to benign tumors [12,13]. The majority (two-thirds) of OSCCs are diagnosed at an advanced stage [14] when prognosis is fairly poor, and the overall 5-year relative survival rate of oral and pharyngeal cancer patients is approximately 59% [15]. Delay in diagnosis can still be considered a major cause of the high morbidity and mortality of OSCC patients. Current standards-of-care (surgery and/or radiotherapy) often end-up with devastating consequences on the appearance and function of affected organs, thereby causing a marked detriment on the quality of life even in successfully treated patients. The molecular mechanism underlying the pathogenesis of OSCC is relatively poorly understood and represents a topic of significant importance. A better understanding of the molecular mechanisms involved in the pathogenesis and progression of the disease is a key to the development of more effective tools to improve early diagnosis of oral cancer, better prognosis, and quality of life of the patients. Discovering new reliable markers for OSCC and developing new diagnostic tools for its early and easy detection is thus a relevant issue in the field of oral pathology research.

Weinberger et al. analyzed molecular differences in protein expression among tumors that arise from different sites of the head and neck region, and they found considerable molecular diversity between different squamous cell carcinomas (SCCs) [16]. In the present study, a proteomic analysis was conducted to analyze the cellular protein profile of a case of G-OSCC and to identify potential signature molecules. Healthy tissue and non-neoplastic epulis tissue were taken as samples for comparison.

2. Materials and methods

2.1. Case report

A 58-year-old female patient reported at the Maxillofacial Unit of the Medical School of the University of Bari (Italy). Intraoral examination revealed the presence of reddish gingival growth at right lower first and second molars measuring approximately 0.5 cm, grade III mobility in the 47 tooth, recession of the marginal gingiva in the region, and generalized chronic periodontitis. Extraoral examination revealed a palpable, nontender, mobile, submandibular lymph node on the right side. On the basis of the above findings, the buccal growth was provisionally diagnosed as an inflammatory/reactive gingival growth and apical periodontitis. Information related to age and gender, smoking, alcohol consumption, clinical aspect of the lesions, and sites of oral involvement were collected. Histopathological analysis of biopsy specimen revealed a malignant neoplasia of epithelial origin, which is characterized by invasive proliferation of nests and cords of neoplastic epithelial cells. Based on histological grading, the tumor was categorized as a well-differentiated G-OSCC.

A case (55-year-old female) of epulis is also included. Epulis is present as a sessile formation on the upper right mucosa gingiva near the front of the mouth between the canine teeth and the first premolar. Its histology is related to fibrosing granulation tissue, firm and rubbery, and pale pink in color.

Sections of the normal buccal mucosa obtained from the two patients were used as the control tissue.

2.2. Reagents

Immobiline DryStrip (pH 3–10 and 4–7, 13 cm), DryStrip, cover fluid, immobilized pH gradient (IPG) buffer, 3-[(3-cholamidopropyl) dimethylammonio]-1-propanesulfonate (CHAPS), bromophenol blue, agarose, acrylamide, tris-base, glycine, sodium dodecyl sulfate (SDS), N,N,N′,N′-tetramethylethylenediamine (TEMED), Coomassie Brilliant Blue R-250, dithiothreitol (DTT), iodoacetamide, acetic acid, and trifluoroacetic acid were purchased from GE Healthcare (Uppsala, Sweden). Sequencing grade-modified trypsin was purchased from Promega (Madison, WI, USA). The remaining chemicals were of analytical grade. All buffers were prepared with Milli-Q water.

2.3. Tissue collection

Normal mucosae tissue, G-OSCC tissue, and epulis tissue were collected with informed consent from the patients at the Maxillofacial Unit of the Medical School of the University of Bari. Inflammatory tissues were sampled from the central part of the inflammatory zone. Cancer samples were obtained from the "core" part of the tumor to avoid the adjacent noncancerous tissue by a standard mapping biopsy strategy. Small fractions of mucosal tissues were carefully removed from the pathological samples. For normal tissue, samples of surface epithelium were obtained selectively by dissection with special care for minimal contamination of nonepithelial cells. All the samples were immediately frozen in liquid nitrogen and stored in a deep freezer (−80 °C) for proteomic analyses. The study was approved by the university ethics committee.

2.4. Sample preparation for proteomic analysis

Proteins were extracted following the protocol reported by Zhang [17]. Briefly, tissue samples of normal, non-neoplastic, and malignant tissues (~200 mg) were ground in small pieces in a mortar with liquid nitrogen, collected in tubes, and homogenized in 2 mL fresh lysis buffer composed of 7 M urea, 2 M thiourea, 40 mM Tris, 4% (w/v) CHAPS, 100 mM DTT, 0.5 mM phenylmethanesulfonyl fluoride (PMSF), 0.5 mM ethylenediaminetetraacetic acid (EDTA), 1% TritonX-100, and 5% IPG buffer. Tissue lysate was further disrupted with an ultrasonic homogenizer and centrifuged at 12,000 × *g* for 10 min at +4 °C. Supernatant was precipitated by the addition of cold acetone (dilution ratio 1:12, v/v) and incubated at −20 °C overnight. After centrifugation at 14,000 × *g* for 15 min at +4 °C, the pellet was resuspended in rehydration buffer. The concentration of the protein extracts was determined by the modified

Bradford method (DC Protein Assay; Bio-Rad, Hercules, CA, USA) [18]. Protein samples were stored at −80 °C.

2.5. Two-dimensional electrophoresis (2-DE)

2-DE was carried out with Amersham Biosystems IPGphor IEF and Ettan Daltsix electrophoresis units according to the protocol previously described [19]. Briefly, 250 μg of tissue-extracted proteins were solubilized in IPG strip rehydration buffer (8 M urea, 2% (w/v) CHAPS, 0.5% IPG buffer, 2% (w/v) DTT, and trace of bromophenol blue) and loaded on 13-cm IPG strips that provided linear pH gradients 3–10 and 4–7. The first pH gradient is suited for an overview pattern of total cell extracts; the second is used to zoom the specific region of the gel (Fig. 1). Isoelectric focusing was carried out at 20 °C by using Ettan Isoelectric Focusing System (GE Healthcare) for a total of 70 kVh. After focusing, the IPG strips were equilibrated for 12 min in the equilibration buffer (50 mM Tris/HCl pH 8.8, 6 M urea, 30% (v/v) glycerol, 2% (w/v), SDS) containing 1% DTT and for 10 min in the same equilibration buffer containing 2.5% iodoacetamide and 0.05% bromophenol blue. For the second dimension, homogeneous SDS-12.5% polyacrylamide electrophoresis gels were used. Electrophoresis was carried out in a Laemmli system [20] at constant current of 15 mA/gel at 10 °C. Molecular weight markers and pI standards were from Bio-Rad. The gels were stained using Coomassie Blue Colloidal dye (Sigma-Aldrich, St. Louis, MO, USA), which enabled quantification of protein staining intensities, allowing quantitative comparison of protein expression levels between the samples.

2.6. Image analysis

Stained gels were scanned with an image scanner (GE Healthcare) at 300 dpi resolution to acquire the gel images that were analyzed using Image-Master 2D Platinum v.6 software (GE Healthcare), which allows quantitative comparison of spot intensity. Relative spot volume (% vol.), i.e., digitized staining intensity integrated over the area of the individual spot divided by the sum of volumes of all spots in the gel and multiplied by 100, was used for spot quantification [21]. The match ID number was used to identify all spots in a match. Spots that were present in all the gels of the three classes of surgical specimens and that showed differences in their relative volume ≥1.7 fold or ≤−1.7 fold with respect to control samples and with $p < 0.05$, using the two-tailed Student t test, were selected for further mass spectrometric analyses (Table 1).

2.7. Protein analysis by nano-ESI-HPLC-MS/MS experiments and database searching

Spots of interest were excised from the 2-DE gels, and in-gel tryptic digestion was carried out following the procedure already described [19].

The obtained tryptic peptides were analyzed by nano-ESI-HPLC-MS/MS using a Q-Exactive™ mass spectrometer (Thermo Fisher Scientific, Waltham, MA, USA) interfaced with an UltiMate 3000 RSLCnano LC system (Thermo Fisher Scientific).

Peptide mixtures were concentrated and desalted on a trapping precolumn (Acclaim PepMap C18, 300 μm × 5 mm nanoViper, 5 μm, 100 Å; Thermo Fisher Scientific), using 0.05% formic acid and 2% acetonitrile at a flow rate of 10 μl/min.

The peptide separation was performed at 35 °C using a C18 column (Acclaim Easy Spray PepMap RSLC C18, 75 μm × 15 cm nanoViper, 3 μm, 100 Å; Thermo Fisher Scientific)with 0.1% formic acid (HCOOH) as eluent A and 80% acetonitrile in 0.08% HCOOH as eluent B, and a linear gradient was established from 4% to 50% B over 30 min, maintained for 6 min, from 50% to 90% B over 1 min, maintained for 10 min before column re-equilibration to 4% B.

Mass spectra were acquired in the m/z range of 350–1600. Data acquisition was performed in a data-dependent Full MS/ddMS^2, enabling the acquisition of MS/MS spectra for the 10 most intense precursor ions (top 10) with a dynamic exclusion of 30 s. Resolution was set to 70.000 for MS spectra acquisition and 17.500 for MS/MS spectra acquisition.

Proteomic analysis was performed using Thermo Proteome Discoverer™ platform (version 2.1.0.81; Thermo Fisher Scientific), interfaced with the SEQUEST HT Search Engine server (University of Washington, USA) used for protein identification. The parameters used for the database searches were as follows: Swiss-Prot human protein database (v2016-04-13) and a contaminant protein database (Contaminantcombinedcontaminant_finalfasta, provided by the manufacturer), trypsin as proteolytic enzyme, up to two missed cleavage, carbamidomethyl as fixed modification for cysteine residues, oxidation of methionine residues and formation of pyroglutamic acid of N-terminal glutamine residues as dynamic modification, 20 ppm mass tolerance for precursor ion and 0.02 Da mass tolerance for MS/MS fragments. Results were filtered for high confident peptides and proteins (False Discovery Rate, 0.01%).

3. Results and discussion

3.1. 2-DE and data analyses

Differential 2-DE analysis of the proteome of G-OSCC tissue samples was performed. Healthy mucosa and a clinically benign epulis lesion were used as control and comparative samples, respectively. Fig. 1A and B show the representative 2-DE gels of the three samples in the pH range 3–10 and 4–7.

Proteomic maps of control, epulis, and G-OSCC samples showed several hundreds of well-resolved protein spots distributed over a wide range of pI values and molecular masses. The overall position and the number of protein spots observed was practically similar in the 2-DE maps of the control (507 ± 24), epulis (489 ± 32), and G-OSCC samples (481 ± 37).

The percentage of matches between gels from the same class and from the three different classes was similar (around 68%) without statistically significant differences between the classes. To reduce the possibility of false positives, only the protein spots systematically present in all the gels of each class were considered in the analysis (Fig. 2).

Image analysis led to highlight spots whose relative volume varied in the 2-DE maps obtained from the analysis of the proteomes extracted from G-OSCC or epulis tissues compared to the control sample. These spots contained differentially expressed proteins that could be related to the pathologic conditions.

In particular, proteins present in 23 spots were overexpressed in the G-OSCC sample (in comparison to the control sample) and 9 of those were also overexpressed in the epulis sample. Moreover, proteins present in 8 spots were underexpressed in the G-OSCC sample and one of those spots was also present in lower amount in the epulis sample with respect to the control sample. Only spot 556 and spot 999, containing vimentin and keratin 13, respectively, exhibited opposite trend in the expression level in the two samples. These results confirmed that epulis tissue showed a lower number of alterations in protein expression level compared to the G-OSCC.

3.2. Protein identification

Protein spots showing significant differences in their volumes in G-OSCC and epulis tissue samples, as compared to normal tissue, were excised from the gels and analyzed by nano-ESI-HPLC-MS/MS experiments. These experiments resulted in the identification of 31 proteins whose expression level was changed in the G-OSCC sample. The expression level of 11 of these proteins was also altered in the epulis sample.

Table 1
Proteins differentially expressed in G-OSCC and epulis tissue compared to control tissues. Proteins are listed according to their spot match identification numbers (ID) as referred in Fig. 1.

Spot ID[a]	Acces. No.[b]	Protein name	Cov.	Pep.	MW[c] [kDa]	pI[d]	Gene ID	Chrom.	Score SEQUEST HT	Categories	Fold change[e]	
											Epul	G-OSCC
342	P55072	Transitional endoplasmic reticulum ATPase	36.228	32	89.77	5.26	VCP	9	200.247997	Protein processing-related proteins	—[f]	+2.17
366	P02679	Fibrinogen gamma chain	27.152	16	51.479	5.62	FGG	4	106.050870	Blood-borne glycoproteins	+3.48	+3.21
433	P20591	Interferon-induced GTP-binding protein Mx1	30.060	23	75.473	5.83	MX1	21	86.2784166	RNA processing-related proteins	—	+5.10
450	P11142-1	Heat shock cognate 71 kDa protein	50.309	34	70.854	5.52	HSPA8	11	689.730728	Stress response-related proteins	+1.91	+2.29
523	P10809	60 kDa heat shock protein, mitochondrial	57.242	34	61.016	5.87	HSPD1	2	324.829026	Stress response-related proteins	—	+2.26
549	P02675	Fibrinogen-beta chain	32.993	14	55.892	8.27	FGB	4	35.3865270	Blood-borne glycoproteins	+10.82	+7.04
556	P08670	Vimentin	74.463	54	53.619	5.12	VIM	10	837.002093	Cytoskeleton structural proteins	−1.72	+2.09
567	P14868	Aspartate–tRNA ligase, cytoplasmic	47.904	22	57.1	6.55	DARS	2	91.2859095	RNA processing-related proteins	—	+2.41
570	P23381	Tryptophan–tRNA ligase, cytoplasmic	46.709	19	53.132	6.23	WARS	14	104.466053	Enzyme	—	+12.42
614	Q8NBS9-1	Thioredoxin domain-containing protein 5	25	9	47.599	5.97	TXNDC5	6	32.0538549	Disulfide isomerase protein	—	−2.20
628	O14745	Na(+)/H(+) exchange regulatory cofactor NHE-RF1	25.419	6	38.845	5.77	SLC9A3R1	17	11.3378964	RNA processing-related proteins	—	−3.70
631	P08670	Vimentin	55.794	26	53.619	5.12	VIM	10	144.882320	Cytoskeleton structural proteins	+1.81	+2.5
647	P08670	Vimentin	48.498	19	53.619	5.12	VIM	10	69.2934554	Cytoskeleton structural proteins	+1.88	+2.10
648	P08670	Vimentin	43.133	15	53.619	5.12	VIM	10	43.7957831	Cytoskeleton structural proteins	—	+2.34
650	P06733-1	Alpha-enolase	75.115	40	47.139	7.39	ENO1	1	1232.58170	Enzyme	—	+1.95
692	P68032	Actin, alpha cardiac muscle 1	42.971	21	41.992	5.39	ACTC1	15	565.164707	Cytoskeleton structural proteins	—	+2.38
696	P60709	Actin, cytoplasmic 1	92	39	41.71	5.48	ACTB	7	2048.53654	Cytoskeleton structural proteins	—	+2.68
700	P29508	Serpin B3	72.051	42	44.537	6.81	SERPINB3	18	897.259493	Cysteine protease inhibitors	—	+5.59
	P48594	Serpin B4	41.538	24	44.825	6.21	SERPINB4	18	320.884156	Cysteine protease inhibitors		
767	O60218	Aldo-keto reductase family 1 member B10	68.0379	22	35.997	7.84	AKR1B10	7	371.111097	Enzyme	—	+13.87
	P52895	Aldo-keto reductase family 1 member C2	35.603	13	36.712	7.49	AKR1C2	10	68.6859819	Enzyme		
	P42330	Aldo-keto reductase family 1 member C3	30.650	13	36.83	7.94	AKR1C3	10	53.3932135	Enzyme		
768	P07355-2	Isof. 2 of Annexin A2	68.907	44	40.386	8.37	ANXA2	15	852.702513	Ca^{2+}- and phospholipid-binding proteins	—	+2.01
	P04083	Annexin A1	54.335	20	38.69	7.02	ANXA1	9	142.948838	Ca^{2+}- and phospholipid-binding proteins		
783	P54920	Alpha-soluble nsf attachment protein	62.712	13	33.211	5.36	NAPA	19	35.0739455	Protein processing-related proteins	—	+5.03
820	P48556	26S proteasome non-ATPase regulatory sub. 8	11.428	5	39.587	7.68	PSMD8	19	18.4493819	Component of the 26S proteasome	+3.80	+1.70
826	Q9Y4E8	Ubiquitin carboxyl terminal hydrolase 15	11.519	8	112.348	5.22	USP15	12	19.6165584	Enzyme	—	−3.74
833	P11476-1	Ras-related protein Rab-1A	57.073	9	22.663	6.21	RAB1A	2	42.0493917	Protein processing-related proteins	—	+2.27
	Q9H0U4	Ras-related protein Rab-1B	46.766	8	22.157	5.73	RAB1B	11	27.1870555	Protein processing-related proteins		
	P20340-1	Ras-related protein Rab-6A	36.538	7	23.578	5.54	RAB6A	11	24.3010213	Protein processing-related proteins		
877	P02647	Apolipoprotein A-I	29.213	7	30.759	5.76	APOA1	11	16.0012671	Lipid-binding proteins	—	−2.98
884	Q01469	Fatty acid-binding protein, epidermal	84.444	16	15.155	7.01	FABP5	8	907.225996	Lipid-binding proteins	—	+2.87
890	P69891	Hemoglobin sub. gamma-1	54.422	8	16.13	7.2	HBG1	11	107.761291	Involved in the oxygen transport	+4.45	+1.93
891	P02042	Hemoglobin sub. delta	46.258	6	16.045	8.05	HBD	11	59.9919946	Involved in the oxygen transport	+5.29	+1.99
933	Q9UBG3	Cornulin	48.889	15	53.502	6.1	CRNN	1	91.2721374	Calcium-binding protein	—	−10.8
999	P13646	Keratin, type I cytoskeletal 13	79.039	42	49.557	4.96	KRT13	17	2575.51624	Cytoskeleton structural proteins	+1.95	−15.47
1009	P13646	Keratin, type I cytoskeletal 13	75.110	729	49.557	4.96	KRT13	17	2186.22087	Cytoskeleton structural proteins	−1.72	−60.56

[a] Spot Identification Number.
[b] Accession Number.
[c] Theoretical molecular weight.
[d] Theoretical isoelectric point.
[e] Fold change in protein expression levels is calculated, for up-regulated protein, as the ratio between the normalized mean volume of each protein spot in the 2-DE maps of G-OSCC and epulis tissue cells and for down-regulated proteins, the normalized mean volume of that protein spot in the 2-DE maps of the control tissue; the negative reciprocal value of this ratio is reported. Only spots exhibiting a fold change ≥ 1.7 or ≤ -1.7 are reported.
[f] The thick horizontal lines indicate no detectable changes in the protein spot volume in epulis with respect to control.

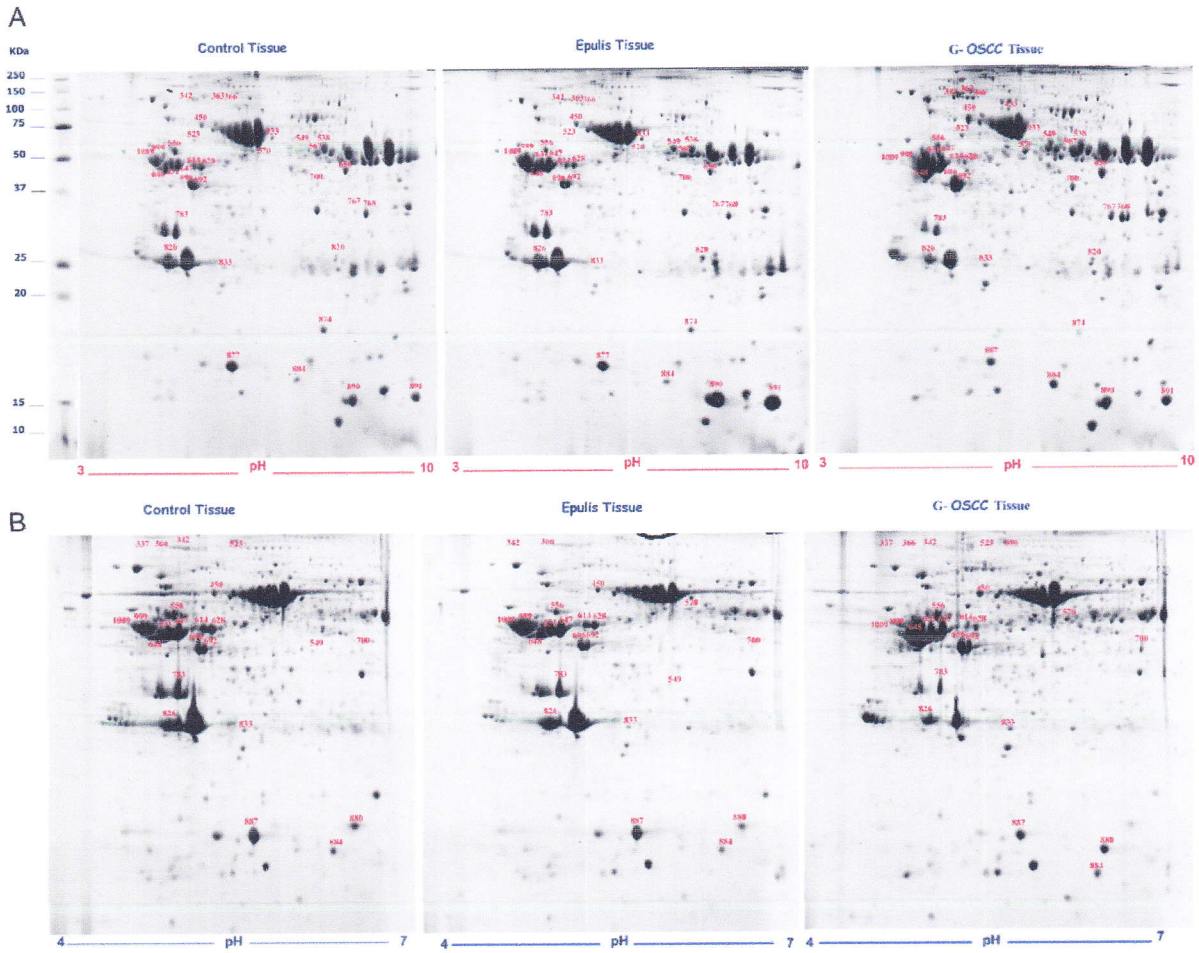

Fig. 1. (A) Representative 2-DE maps of the total protein extracts from control, epulis, and G-OSCC tissue samples (linear IPG pH 3–10). Protein spots that show different relative volumes in the G-OSCC and epulis samples compared to the control sample were indicated by match ID number. Proteins present in these spots were identified by nano-ESI-HPLC-MS/MS analysis and database search and are listed in Table 1. (B) Representative 2-DE maps of the total protein extracts from control, epulis, and G-OSCC tissue samples (linear IPG pH 4–7). Protein spots that show different relative volumes in the G-OSCC and epulis samples compared to the control sample, were indicated by match ID number. Proteins present in these spots were identified by nano-ESI-HPLC-MS/MS analysis and database search and are listed in Table 1.

In particular, fibrinogen gamma chain (spot 366), heat shock cognate 71 kDa (spot 450), fibrinogen beta chain (spot 549), 26S proteasome non-ATPase regulatory protein (spot 820), hemoglobin subunit gamma 1 (spot 890), and hemoglobin subunit delta (spot 891) were significantly up-regulated in both G-OSCC and epilis (Table 1).

Notably, proteomic studies of epulis tissues are still scarce; hence, the present study might provide first insights on this inflammatory status also in relation to G-OSCC development.

In G-OSCC, a 14-fold increased expression of members of the Aldo-keto reductase family (AKR), AKR-1-B10, AKR-1-C2, and AKR-1-C3, was detected. The AKR enzymes reduce a variety of aldehydes and/or ketones to their corresponding alcohols using NADH or NADPH [22] and are involved in intracellular detoxification and carcinogenesis processes [23–26]. Enhanced expression of AKR-1-B10 has been detected in many types of tumors [23,24]. Silencing of the AKR-1-B10 gene was found to inhibit growth of colorectal cancer [27] and SCC [28]. AKR-1-C2 appears to be associated with disease progression in prostate cancer [29].

The expression level of tryptophan-tRNA ligase, cytoplasmic tryptophan aminoacil t-RNA synthase (WARS), was also significantly increased (12-fold) in G-OSCC, thus confirming recently published results that, in addition to its well-characterized angiostatic function in endothelial cells, reported a key role of this protein in OSCC progression and invasiveness [30].

The large overexpression of the three members of the AKR family proteins and of WARS in G-OSCC is likely involved in the development and progression of this oral cancer. As the amount of these proteins was not altered in the epulis tissue (compared to the control sample, see Table 1), these proteins could be regarded as specific biomarkers for monitoring the development of this tumor. Among the protein processing-related proteins, about five-fold increase was observed in the expression level of alpha-soluble NSF attachment protein (α-SNAP) and RAS-related proteins, RAB-1A, RAB-1B and RAB-6A, in the G-OSCC extract. In recent years, critical roles of α-SNAP [31] and Rab GTPases [32] in tumor development and their recognition as potential therapeutic targets have emerged.

In particular, a recent proteomic study also identified a Ras-related protein, Rab-2A isoform (RAB2A), as a signature protein of OSCC and found the protein to be overexpressed in OSCC [33]. About five-fold increase of Serpin B3 and Serpin B4 levels was also found in the G-OSCC sample. Elevated expression of these serine/cysteine protease inhibitors is reported to contribute to cancer development [34]. G-OSCC tissue extracts showed, however, decrease in the expression level of proteins like ubiquitin carboxyl-terminal hydrolase (USP1), apolipoprotein A1 (APOA1), Na^+/H^+ exchange regulatory cofactor NHE-RF1 (SLC9A3R1), and in particular cornulin (CRNN) and keratin-type cytoskeletal 13 (CRKT13).

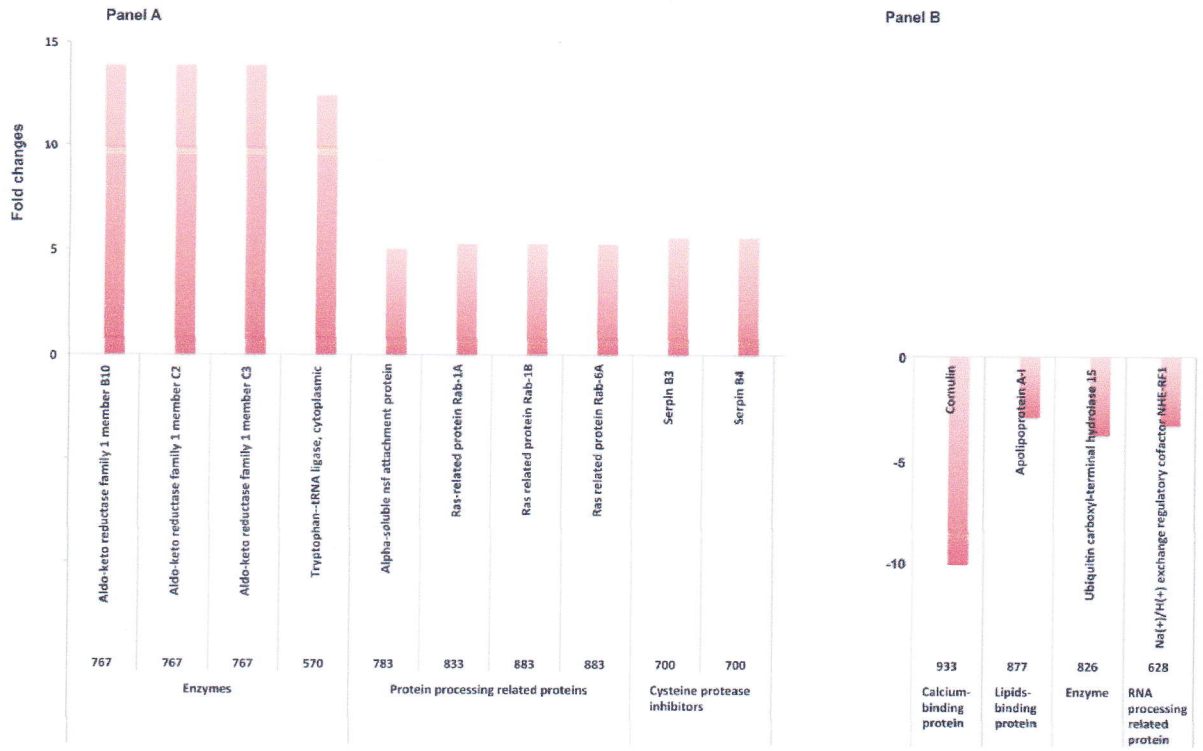

Fig. 2. Diagram of changes in the expression level of proteins in the G-OSCC tissue extract (positive- or negative-fold changes in their relative spot volume) with respect to the control sample.

CRNN, which belongs to the protein family forming the cornfield cell envelope, is an important barrier of the mucosa and skin. It is a survival factor that participates in the clonogenity of squamous esophageal epithelial cell line [35].

It has been reported that the expression level of CRNN was downregulated in some cancers and, in particular, in OSCC [35]. Worth stressing, this protein exhibited an inhibitory function in regulating cell proliferation probably due to a block in the cell cycle, thus suggesting that this protein may play a role in OSCC progression [36].

Keratins are the intermediate filament-forming proteins of epithelial cells that have an important role in cell protection from mechanical and non-mechanical stressors [37,38]. Several studies have provided evidence for alteration of keratin expression in squamous tumor tissue of the oral cavity and their involvement in tumorigenesis regulation, cancer cell invasion, and metastasis [39–43]. These findings suggest that keratins may have a role as diagnostic tumor markers [44]. The expression levels of CRNN and CRKT13 were also found to be significantly decreased in preneoplastic tumors with a high risk of malignant progression [45].

In conclusion, the present study showed that proteomic analysis of G-OSCC tissue enabled the identification of putative biomarkers such as aldo-keto reductase enzymes (AKR-IBIO, AKR-IC3, and AKR-I C2), tryptophan-tRNA ligase cytoplasmic (WARS), cornulins (CRNN), and keratin type I cytoskeletal 13 (KRT13) that could be useful to monitor OSCC development. These results could also be relevant in developing specific diagnostic tools suitable to discriminate G-OSCC tissues from epulis tissues for the early diagnosis of this pathology.

Acknowledgement

F.P. was supported by a research grant from the University of BARI.

Appendix A. Supplementary data

Supplementary data associated with this article can be found, in the online version, at https://doi.org/10.1016/S1348-8643(17)30044-7.

References

[1] Petersen PE. Oral cancer prevention and control – the approach of the World Health Organization. *Oral Oncol* 2009;45:454–60.
[2] Bertolus C, Goudot P, Gessain A, et al. Clinical relevance of systematic human papillomavirus (HPV) diagnosis in oral squamous cell carcinoma. *Infect. Agents Cancer* 2012;7:13.
[3] Johnson NW, Jayasekara P, Amarasinghe AA. Squamous cell carcinoma and precursor lesions of the oral cavity: epidemiology and aetiology. *Periodontol 2000* 2011;57:19–37.
[4] Estilo CL, O-charoenrat P, Talbot S, et al. Oral tongue cancer gene expression profiling: identification of novel potential prognosticators by oligonucleotide microarray analysis. *BMC Cancer* 2009;2:9–11.
[5] Boy SC. Leukoplakia and erythroplakia of the oral mucosa—a brief overview. *SADJ* 2012;67:558–60.
[6] Feller L, Lemmer J. Oral squamous cell carcinoma: epidemiology, clinical presentation and treatment. *J Cancer Ther* 2012;3:263–8.
[7] Mahomed F. Oral submucous fibrosis—a potentially malignant condition of growing concern. *SADJ* 2012;67:4–5.
[8] Scully C, Bagan J. Oral squamous cell carcinoma overview. *Oral Oncol* 2009;45:301–8.
[9] Van der Waal I. Potentially malignant disorders of the oral and oropharyngeal mucosa; terminology, classification and present concepts of management. *Oral Oncol* 2009;45:317–23.
[10] Wallace ML, Neville BW. Squamous cell carcinoma of the gingiva with an atypical appearance. *J Periodontol* 1996;11:1245–8.
[11] Feller L, Wood NH, Khammissa RA, et al. Human papillomavirus-mediated carcinogenesis and HPV-associated oral and oropharyngeal squamous cell carcinoma. Part 1: human papillomavirus-mediated carcinogenesis. *Head Face Med* 2010;6:14.
[12] Fukuda M, Kusama K, Sakashita H. Molecular insights into the proliferation and progression mechanisms of the oral cancer: strategies for the effective and personalized therapy. *Jpn Dent Sci Rev* 2012;48:23–41.
[13] Ralhan R. Diagnostic potential of genomic and proteomic signatures in oral cancer. *Int J Hum Genet* 2007;7:57–66.
[14] McGurk M, Chan C, Jones J, et al. Delay in diagnosis and its effect on outcome in head and neck cancer. *Br J Oral Maxillofac Surg* 2005;43:28–34.

[15] Jemal A, Siegel R, Ward E, et al. Cancer statistics 2007. *CA Cancer J Clin* 2007;57:43–66.
[16] Weinberger PM, Merkley M, Lee JR, et al. Use of combination proteomic analysis to demonstrate molecular similarity of head and neck squamous cell carcinoma arising from different subsites. *Arch Otolaryngol Head Neck Surg* 2009;135:694–703.
[17] Zhang H, Guo H, Fan Q, et al. Analysis and identification of tumor marker in lung cancer using two-dimensional gel electrophoresis and matrix-assisted laser desorption ionization time of flight mass spectrometry. *Life Sci J* 2009;3:46–53.
[18] Bradford MM. A rapid and sensitive method for the quantitation of microgram quantities of protein utilizing the principle of protein-dye binding. *Anal Biochem* 1976;72:248–54.
[19] Lippolis R, Siciliano RA, Pacelli C, et al. Altered protein expression pattern in skin fibroblasts from parkin-mutant early-onset Parkinson's disease patients. *Biochim Biophys Acta* 2015;1852:1960–70.
[20] Laemmli UK. Cleavage of structural proteins during the assembly of the head of bacteriophage T4. *Nature* 1970;227:680–5.
[21] Appel RD, Hochstrasser DF. Computer analysis of 2-D images. *Methods Mol Biol* 1999;112:363–81.
[22] Cao D, Fan ST, Chung SS. Identification and characterization of a novel human aldose reductase-like gene. *J Biol Chem* 1998;273:11429–35.
[23] Hyndman D, Bauman DR, Heredia VV, et al. The aldo-keto reductase superfamily homepage. *Chem Biol Interact* 2003;144:621–31.
[24] Jin J, Krishack PA, Cao D. Role of aldo-keto reductases in development of prostate and breast cancer. *Front Biosci* 2006;11:2767–73.
[25] Saraswat M, Mrudula T, Kumar PU, et al. Overexpression of aldose reductase in human cancer tissues. *Med Sci Monit* 2006;12:CR525–9.
[26] Takahashi M, Fujii J, Miyoshi E, et al. Elevation of aldose reductase gene expression in rat primary hepatoma and hepatoma cell lines: implication in detoxification of cytotoxic aldehydes. *Int J Cancer* 1995;62:749–54.
[27] Yan R, Zu X, Ma J, et al. Aldo-keto reductase family 1 B10 gene silencing results in growth inhibition of colorectal cancer cells: implication for cancer intervention. *Int J Cancer* 2007;121:2301–6.
[28] Miller VL, Lin HK, Murugan P, et al. Aldo-keto reductase family 1 member C3 (AKR1C3) is expressed in adenocarcinoma and squamous cell carcinoma but not small cell carcinoma. *Int J Clin Exp Pathol* 2012;5:278–89.
[29] Huang KH, Chiou SH, Chow KC, et al. Overexpression of aldo-keto reductase 1C2 is associated with disease progression in patients with prostatic cancer. *Histopathology* 2010;57:384–94.
[30] Lee CW, Chang KP, Chen YY, et al. Overexpressed tryptophanyl-tRNA synthetase, an angiostatic protein, enhances oral cancer cell invasiveness. *Oncotarget* 2015;6:21979–92.
[31] Andreeva AV, Kutuzov MA, Voyno-Yasenetskaya TA. A ubiquitous membrane fusion protein alpha SNAP and RAB GTPases: a potential therapeutic target for cancer, diabetes and neurological disorders? *Expert Opin Ther Targets* 2006;10:723–33.
[32] Recchi C, Seabra MC. Novel functions for Rab GTPases in multiple aspects of tumour progression. *Biochem Soc Trans* 2012;40:1398–403.
[33] Sun Y, Sheshadri N, Zong WX. SERPINB3 and B4: From biochemistry to biology. *Semin Cell Dev Biol* 2017;62:170–7.
[34] Contzler R, Favre B, Huber M, et al. Cornulin, a new member of the fused gene family, is expressed during epidermal differentiation. *J Invest Dermatol* 2005;124:990–7.
[35] Imai FL, Uzawa K, Nimura Y, et al. Chromosome 1 open reading frame 10 (C1orf10) gene is frequently down-regulated and inhibits cell proliferation in oral squamous cell carcinoma. *Int J Biochem Cell Biol* 2005;37:1641–55.
[36] Kai C, Yan L, Yongdong D, et al. Characterization of tumor suppressive function of cornulin in esophageal squamous cell carcinoma. *PLoS One* 2013;8(7):e68838.
[37] Bragulla HH, Homberger DG. Structure and functions of keratin proteins in simple, stratified, keratinized and cornified epithelia. *J Anat* 2009;4:516–59.
[38] Coulombe PA, Omary MB. 'Hard' and 'soft' principles defining the structure, function and regulation of keratin intermediate filaments. *Curr Opin Cell Biol* 2002;14:110–22.
[39] Kainuma K, Katsuno S, Hashimoto S, et al. Differences in the expression of genes between normal tissue and squamous cell carcinomas of head and neck using cancer-related gene cDNA microarray. *Acta Otolaryngol* 2006;126:967–74.
[40] Chi LM, Lee CW, Chang KP, et al. Enhanced interferon signaling pathway in oral cancer revealed by quantitative proteome analysis of microdissected specimens using 16O/18O labeling and integrated two-dimensional LC-ESI-MALDI tandem MS. *Mol Cell Proteomics* 2009;8:1453–74.
[41] Ohkura S, Kondoh N, Hada A, et al. Differential expression of the keratin-4, -13, -14, -17 and transglutaminase 3 genes during the development of oral squamous cell carcinoma from leukoplakia. *Oral Oncol* 2005;41:607–13.
[42] Matthias C, Mack B, Berghaus A, et al. Keratin 8 expression in head and neck epithelia. *BMC Cancer* 2008;8:267.
[43] Moll R, Divo M, Langbein L. The human keratins: biology and pathology. *Histochem Cell Biol* 2008;6:705–33.
[44] Karantza V. Keratins in health and cancer: more than mere epithelial cell markers. *Oncogene* 2011;2:127–38.
[45] Schaaij-Visser TB, Graveland AP, Gauci S, et al. Differential proteomics identifies protein biomarkers that predict local relapse of head and neck squamous cell carcinomas. *Clin Cancer Res* 2009;15:7666–75.